TECHNICAL MEMORANDUM

223

ECMWF TOGA COARE dataset

E. Klinker and A. Hollingsworth

Research Department

August 1996

European Centre for Medium-Range Weather Forecasts
Europäisches Zentrum für mittelfristige Wettervorhersage
Centre européen pour les prévisions météorologiques à moyen

ABSTRACT

Real-time data available in the ECMWF operational assimilation system during the TOGA-COARE experiment has improved the description of the flow in the warm pool area. Diagnostic output from additional short range integrations with a T106/L31 version of the ECMWF model based on these high quality initial conditions provide a comprehensive archive (with 6-hourly frequency) of the diabatic and adiabatic tendencies during the Intensive Observation Period (IOP). The diabatic tendencies can be compared with corresponding estimates of the different physical processes made directly from field data. In this note we use this archive to document basic aspects of diabatic processes in the TOGA COARE area, as simulated in the course of the assimilation.

1. INTRODUCTION

The scientific objectives of the atmospheric component of the TOGA/COARE experiment include:

* Determination of the synoptic and mesoscale components of the large-scale slowly varying atmospheric circulation in the warm pool, including in particular the morphology of the moist-convective stage of the 30-60 day mode and its sub-components.

* Determine the relationship of the phenomena described above to the heat, moisture, and momentum fluxes at the ocean atmosphere interface, in an attempt to relate the atmospheric phenomena of the western Pacific Ocean to transitions in the dynamics and thermodynamics of the upper-ocean structure.

* Determine the morphology of episodic westerly burst phenomena including their sources whether *in-situ* or remote.

* Determine the vertical heating distribution and life cycles associated with synoptic events and mesoscale convective cluster components, and compare these results to other regions in the tropics.

These issues play a key role in the formulation and validation of atmospheric models for weather prediction and for climate simulation. A special effort was made in the course of the experiment to provide a subset of the COARE observations to operational Centre's via the WMO GTS. Those data were included in the real-time operational assimilation at ECMWF and other forecast centres.

In this note we use products from the operational assimilation and from additional model runs to calculate the three-dimensional diabatic forcing (with 6-hourly frequency) during the TOGA COARE experiment. Our main aim is to stimulate interest in comparisons of the field measurements with the model-based estimates from a state of the art assimilation system. In section 2 we describe the assimilation system and the real-time TOGA COARE data used in the assimilation. In section 3 we describe the mean large-scale flow field during the major part of the Intensive Observation Period (IOP) November 92 to February 93, and describe the spatial distribution

of the associated diabatic fields and surface fluxes. In section 4 we illustrate the three dimensional fields of diabatic and adiabatic tendencies in the temperature, humidity, and momentum fields. Finally in Section 5, we discuss the internal consistency of the results, and their short-comings. We also discuss lines of further investigations.

2. DATA ASSIMILATION SYSTEM

The mass and wind analysis used in the operational data assimilation at ECMWF during the TOGA COARE experiment is based on the multi-variate optimum interpolation (OI) scheme (*Lorenc*, 1981). Further developments of the ECMWF assimilation system (some are described by *Lönnberg*, 1988; *Undén*, 1988) in the late 80's and early 90's include the use of divergent structure functions, the increase of the effective horizontal and vertical resolution and the use of the first guess at the appropriate time. The model version as part of the operational data assimilation was the T213 spectral model with 31 levels in the vertical.

During the TOGA COARE IOP a large number of additional observations were received in time to include them into the real-time assimilation system. In particular a high percentage of sonde data was received for 0z and 12z, whereas only a small number of observations form 6z and 18z where included as input data for the operational analysis. Fig 2.1 shows an example of the data monitoring statistics for January 1993 in the TOGA COARE area. For the evaluation in the Intensive Flux Array (IFA) it is important to notice that for a 10 by 10 degree box covering the IFA on average 8 sondes per day were available in the analysis (Fig 2.1b).

3. THE MEAN LARGE-SCALE FLOW

In this section we describe the time-mean large-scale flow field in the central and western tropical Pacific for the three month period December 92 to February 93.

3.1 **The Time-Mean Flow Variables**

Figs 3.1a and 3.1c shows the DJF 200mb and 850 mb mean wind field in the Western Pacific. At 850 mb (Fig 3.1c), the north-east trades have peak winds of 10 m/s at 10N between 140E and 160E. The 5m/s isotach is almost parallel to the equator at about latitude 5N. The south-east trades hardly extend to 15S. Between northern Australia and latitude 5N, the 850 mb winds are westerly with speeds up to 5 m/s. The 850 mb westerlies extend eastward to the dateline. The main features on the 200mb wind field (Fig 3.1a) are the sub-tropical jets. The 10 m/s isotach for the westerly jet lies along 17S in the Southern Hemisphere. In the NH the corresponding isotach lies along 17N between 120E and 180E, and then arcs southeastward to cross the equator at 145W. In the tropical region the 200 mb wind is mainly easterly to the west of the dateline, and southerly or south-westerly to the east of the dateline.

Figs 3.1b and 3.1d show the divergent component of the mean wind at 200 and 850 mb. At 200 mb the main divergence occurs along the ITCZ in a band oriented along 7S between 120E and 180E. East of the dateline the upper-level divergence maximum is oriented towards the south east along the south Pacific convergence zone (SPCZ). The largest divergent winds at 200 mb, in excess of 6 m/s southerly, occur in a band along 10N between 140E and 180E. At 850 mb, the maximum divergent winds (in excess of 2 m/s northerly) occur in about the same location.

Fig 3.2 provides latitude-height cross-sections of the mean u,v, q and ω fields, averaged over the band of longitude from 140E to 170E. The dominant tropical tropospheric features in the zonal wind cross-section (Fig 3.2a) are the band of easterlies north of the equator, sloping upward and southward, and the band of westerlies south of the equator, again sloping upwards and southwards, with low-level winds in excess of 5 m/s below 700 mb. The Southern Hemisphere easterlies are confined to an area south of 15S. The mean meridional wind (Fig 3.2b) shows that the strongest poleward and equatorward flows in the local Hadley circulation occur in the winter hemisphere, with mean southerlies in excess of 4 m/s in the upper troposphere and mean northerlies in excess of 3m/s in the lower troposphere. In the Southern Hemisphere, the mean upper-level poleward component just exceeds 1 m/s. The cross-section of the mean field (Fig 3.2d) shows mean subsidence to the north of 10N. There is mean ascent from 8N to 22S, with a broad peak between 5N and 5S, and a secondary peak at 15S. The only note-worthy feature on the q cross-section (Fig 3.2c) is that the specific humidity between 400 and 500mb is highest in the area of mean ascent in the Hadley cell. The temperature cross-section (not shown) is even more featureless.

3.2 The Time-Mean Diabatic Fields

Fig 3.3a shows the estimated mean precipitation P for the period, based on the precipitation in the first 24 hrs of the operational forecasts. The main features are the east-west oriented maximum (with values up to 20 mm/day) in the ITCZ north of the equator, the NW-SE oriented maximum in the SPCZ which extends across the equator to the NH maximum, the local maxima over the islands of the maritime continent and on the NW coast of Australia and, finally, an isolated local maximum of 20 mm/day at (160E, 4S), in the TOGA/COARE area. Fig 3.c shows the mean evaporation, E, for the period. There is a broad maximum north of the equator with peak values of 8 mm/day at 15N. A minimum of 4-5 mm/day extends along the equator, with values of 4-5 mm/day in the COARE area. The peak values in the SH are of order 6 mm/day. Fig 3.3c shows P-E, the net gain in water for the surface (equivalent to a loss for the atmosphere) mainly in the tropical convergence zone and a loss for the surface in the trade wind areas. Fig 3.4d shows the mean vertical velocity (Pa/s) with rising areas shaded. There is a striking degree of correspondence between the distribution of mean vertical velocity and of mean precipitation.

We now consider the energy budget of the TOGA COARE area. Following *Fortelius and Holopainen* (1990) the vertically integrated diabatic heating Q_{dry} for a lat-lon box of atmosphere (extending from the surface to the top of the atmosphere) can be written as

$$Q_{dry} = R_a + L.P + H$$

where R_a is the net radiative heating of the atmosphere, L is the latent heat of vaporization of water, and P is the precipitation rate, and H is the surface sensible heat flux; this equation assumes that the vertically integrated frictional heating is negligible. The corresponding diabatic moisture change can be expressed in energy units as

$$Q_{wet} = L.\,(E - P)$$

where E is the evaporation rate.

The energy balance of the surface reads

$$R_e = H + L.E + B$$

where R_e is the net radiation at the surface, and B is the flux into the underlying material.

Thus

$$Q = Q_{dry} + Q_{wet} = R_a + R_e - B = R - B$$

where R is the net radiation at the top of the atmosphere.

Terms in the Radiative Budget

Fig 3.4 provides plots of the various terms in the radiative budget. Fig 3.4a is a plot of R, the net radiation at the top of the atmosphere, with a positive sign indicating a gain for the atmosphere. The main feature of this field is a net gain for the atmosphere of about 100 Wm^{-2} at 30S which decreases steadily to zero at about 10N and to a net loss of about -50 Wm-2 at 30N.

Fig 3.4b is a plot of R_a, the net radiative heating/cooling of the atmosphere. This term is negative everywhere with peak values in excess of -150 Wm^{-2} in the subsidence areas along 20N, and peak values in excess of -125 Wm^{-2} on the equator at 175E, and along 20S. Minimum values of -75 Wm^{-2} or less occur in the main ascent regions, because the long wave cooling occurs at much lower (cloud top) temperatures, and is partly offset by short wave absorption in clouds.

Fig 3.4c shows the net radiation at the surface, R_e, with the negative sign indicating a loss to the atmosphere. The largest radiative input into the ocean is seen at about 25S with values in excess of -225 Wm^{-2}. There is also a distinct local maximum of -125 Wm^{-2} along 10N, just to the north of the main precipitation area.

Fig 3.4d shows the OLR (outgoing longwave radiation), with maxima of -275 Wm^{-2} in the subsidence regions, and minima of -225 Wm^{-2} in the main ascent regions.

The Overall Energy Budget

Fig 3.5a is a plot of the latent heat flux, with positive values again meaning a gain for the atmosphere. The values range from 225 Wm^{-2} in the sub-tropics over the oceans, to a minimum of about 125 Wm^{-2} in the equatorial region. Fig 3.5c shows that the sensible heat flux has comparatively large values of up to 125 Wm^{-2} over land but only negligible ones in the area of interest over the ocean. Therefore the sum of the turbulent surface fluxes (Fig 3.5c) has a fairly smooth transition from land to ocean values.

Finally, Fig 3.5b shows Q, the net gain in energy in the atmospheric column, that must be balanced by horizontal transport processes in the atmosphere, typically by transport to higher latitudes. This shows peak values of 125 Wm^{-2} in the main ascent region along 7N, and up to 100 Wm^{-2} in the SPCZ.

4. THREE-DIMENSIONAL DIABATIC FORCING

For a period of three months including 15 November 1992 to 15 February 1993 additional short range forecasts have been run to provide a 3-dimensional picture of the diabatic forcing during TOGA COARE. As the normal post-processing for the high resolution model (T213) provides only boundary fluxes from the output of the parametrization schemes, a lower horizontal resolution (T106) version of the model with extended diagnostic capabilities has been used to extract 3-dimensional diabatic and dynamic tendencies without stretching the computer requirements too much. Short-range model integrations in this full diagnostic mode were run from the 6-hourly available analyses and the diabatic forcing for all major prognostic parameters (temperature, humidity and momentum) were post-processed.

Fig 4.1 provides an overview of the variability of the diabatic forcing in the warm pool area. The zonal wind (a) and the diabatic heating due to cumulus convection (b) averaged over the TOGA COARE area (150-160E) are shown as a time-pressure diagram for a period of three months starting 15 November 1992. Strong diabatic heating from the dominating process of cumulus convection occurs during the second half of December, accompanied by comparatively strong westerly wind bursts of more than 10 m/s. A similar but less intensive event can be found at the beginning of February.

The vertical structure of the main components of the diabatic forcing is shown in Figs 4.2 to Fig. 4.4. The mean values of short range forecasts (6 hours) started from all four available analysis of each day represent zonal averages over the TOGA COARE area and a time average over the third week of December 1992. The heat budget (Fig 4.2) shows the dominance of the cumulus convection above the boundary layer with a maximum

between 500 and 400 hPa. The melting level emerges as a sharp gradient of the heating between 600 and 700 hPa. The larger heating rates around 3 degrees south compared to the secondary maximum around 4 degrees north correspond to a much deeper convective process south of the equator as well, as can be seen in particular for the cumulus condensation part in the humidity budget (Fig 4.3). The budget for the zonal momentum (Fig 4.4) is again dominated by a process related to the cumulus convection. Large values of the cumulus momentum exchange are found in areas of large vertical wind shear and intense convective processes.

5. DISCUSSION

The above estimates of the components of the energy budget are generally consistent with current knowledge. However it is of interest to compare them with estimates made directly from in-situ data during the TOGA-COARE experiment. Preliminary results from observational studies seem to suggest that there is a fair amount of agreement between model results and observationally based estimates. One interesting difference has already emerged, which shows that the rather sharp gradient of the diabatic heating profile close to the melting level around 600 hPa is not found from observations. This could be an indication of the missing process of mesoscale downdraughts in the model that would distribute the cooling over a deeper layer below the melting level.

The rather incomplete use of TOGA COARE observational data in the real-time operational analysis requires a re-analysis for the full period. As the TOGA COARE IOP is part of the official ECMWF re-analysis period it is planned to rerun the diagnostic integrations from the re-analysis files that have a horizontal resolution of T106. Further improved analysis schemes will be tested in re-analysis experiments for shorter periods using the thee-dimensional variational analysis.

REFERENCES

Fortelius, C and E Holopainen, 1990: Comparison of energy source estimates derived from atmospheric circulation data with satellite measurements of net radiation. Journal of Climate, **3**, 646-660.

Lönnberg, P, 1988: Developments in the ECMWF analysis system. Proceedings of the ECMWF Seminar on data assimilation and the use of satellite data. 5-9 September 1988. Volume I.

Lorenc, A 1981: A global three-dimensional multivariate statistical interpolation scheme. Mon Wea Rev, **109**,701-721.

Undén, P, 1989: Tropical data assimilation and analysis of divergence. Mon Wea Rev , **117**, 2495-2517.

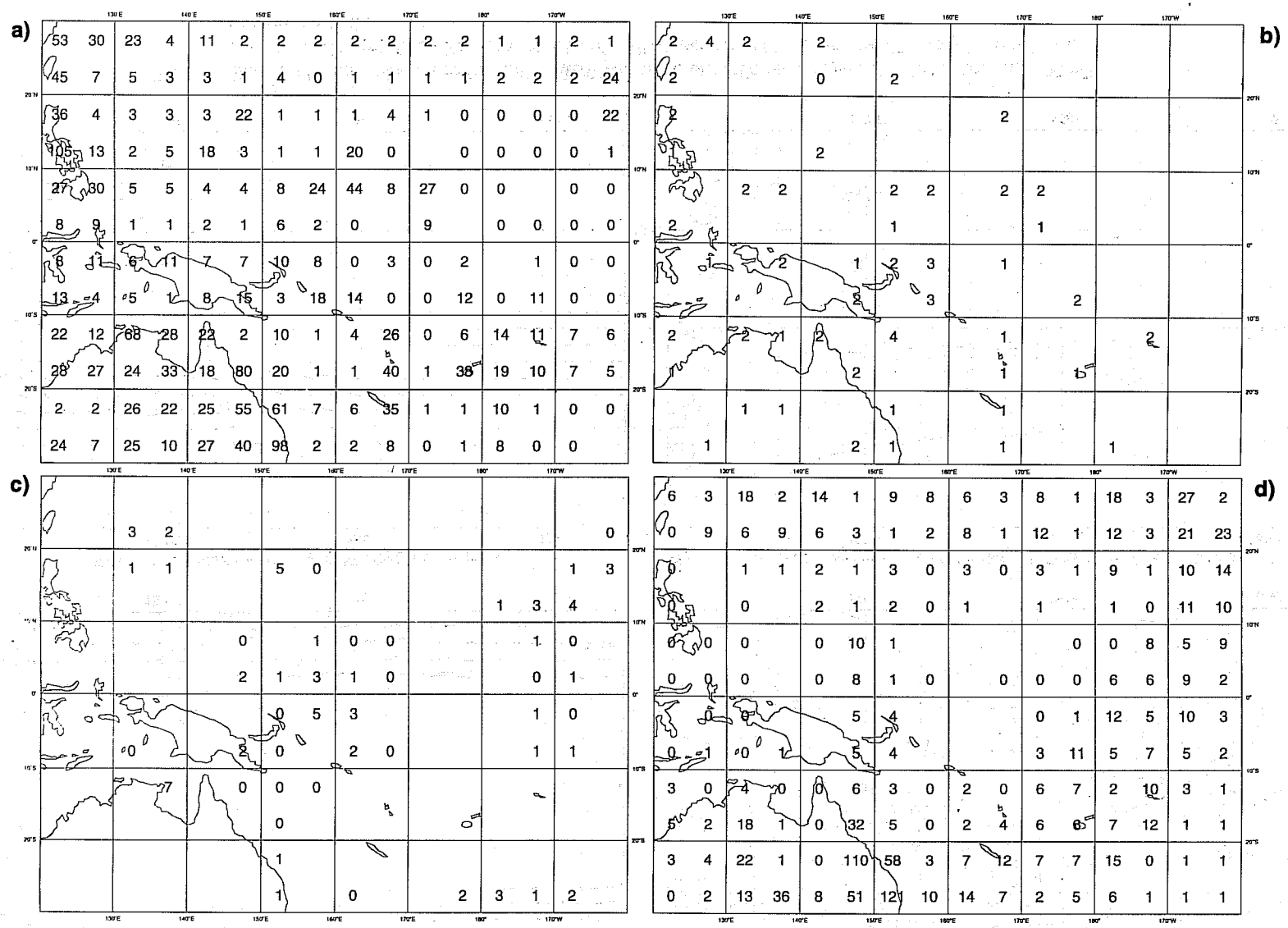

Fig 2.1 ECMWF monitoring statistics of observational data for January 1993 in the TOGA COARE area. Land and ship based SYNOP's (a), sondes reporting 500 hPa height (b), drifting buoys (c), aircraft wind observations between 300 and 150 hPa (d). Numbers represent average 24 hour availability for 5 by 5 degree boxes.

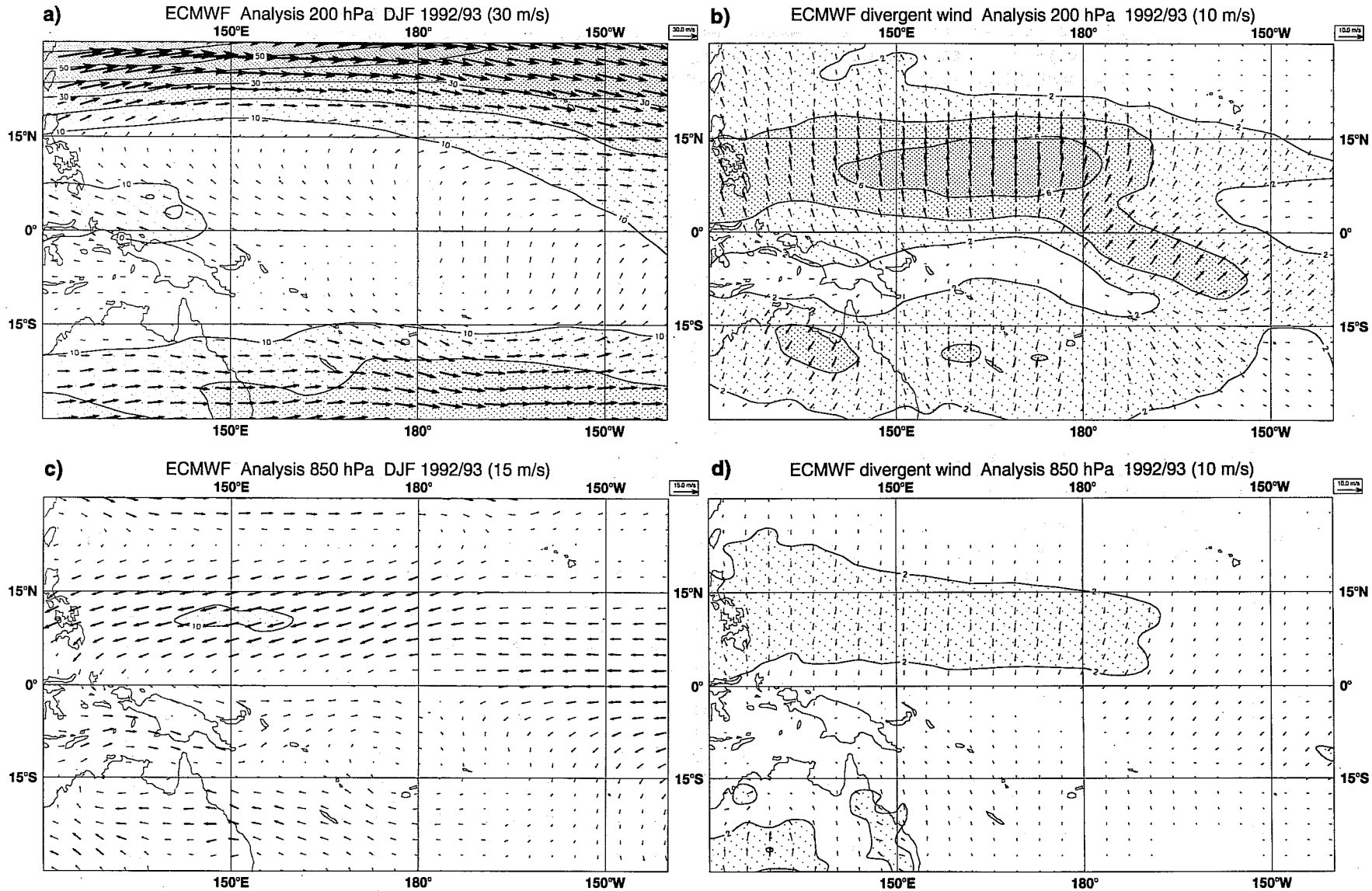

Fig 3.1 Seasonal mean wind fields for DJF 1992/93 from the operational analysis. 200 hPa wind (a), 200 hPa divergent wind (b), 850 hPa wind (c), 850 hPa divergent wind (d). Units are; 30 m/s (a), 10 m/s (b), 15 m/s (c), and 10 m/s (d)

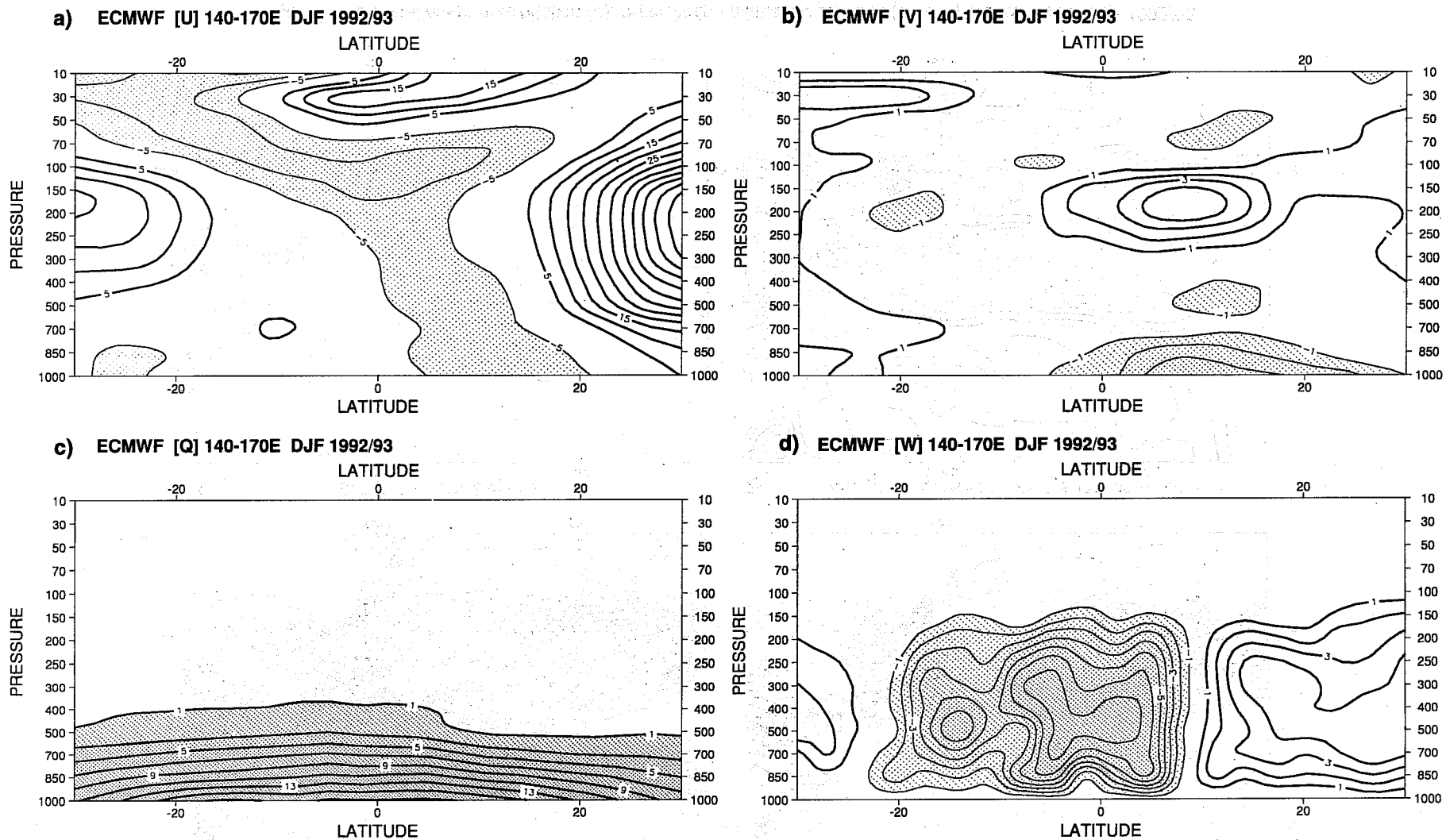

Fig. 3.2 Latitude-height cross sections of seasonal mean fields for DJF 1992/93 from the operational analysis. All fields are averaged in longitudinal direction from 140E to 170E. Zonal wind (a), meridional wind (b), specific humidity (c), and vertical velocity (d). Units: m/s in (a) and (b), g/kg (c), 10^{-2} Pa/s (d).

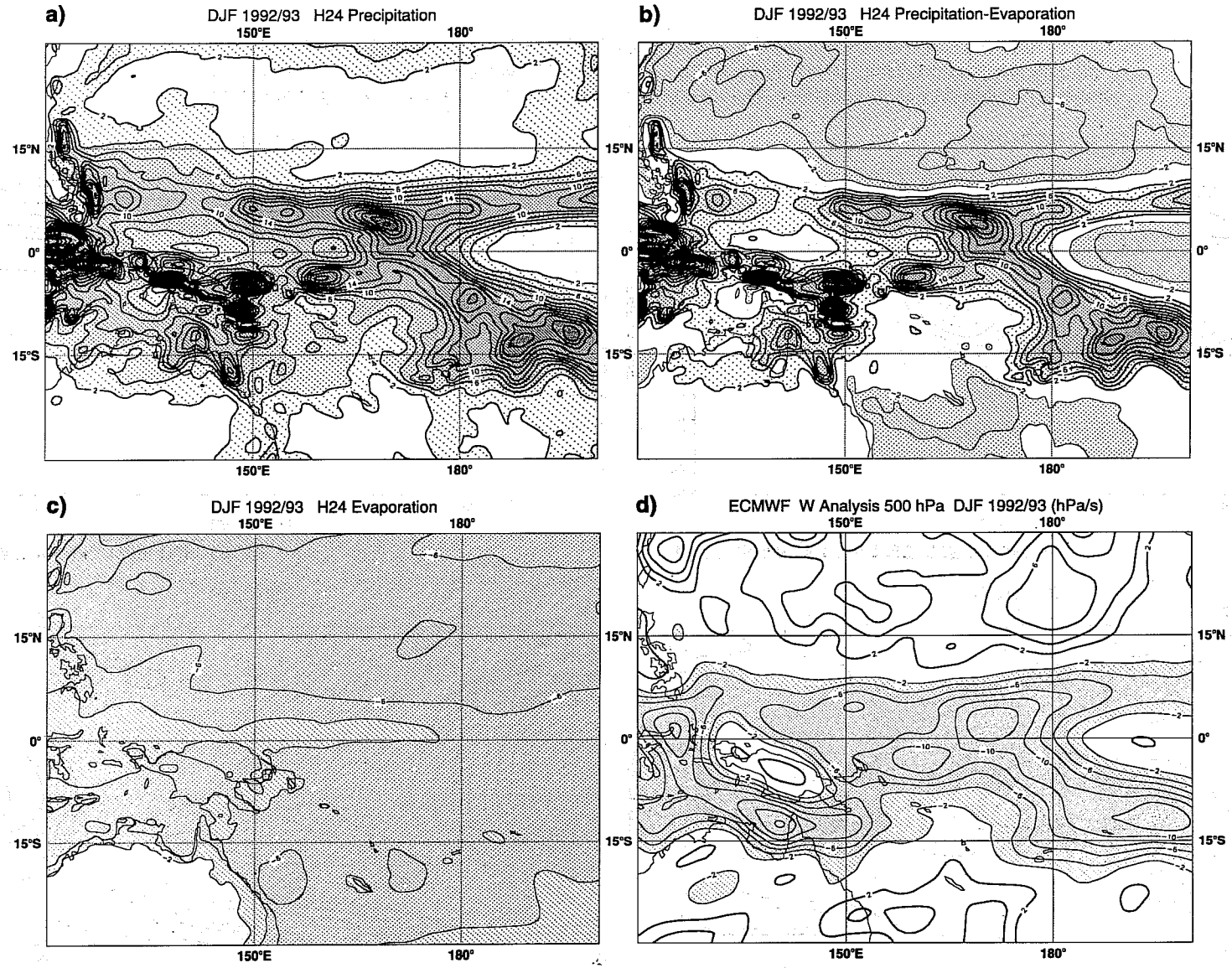

Fig. 3.3 Seasonal mean precipitation (a), precipitation minus evaporation (b), evaporation (c) for DJF 1992/93 accumulated over the first 24 hours of the operational forecasts. Seasonal mean vertical velocity for DJF 1992/93 at 500 hPa (d). Units: mm/day for (a-c) and hPa/s for (d).

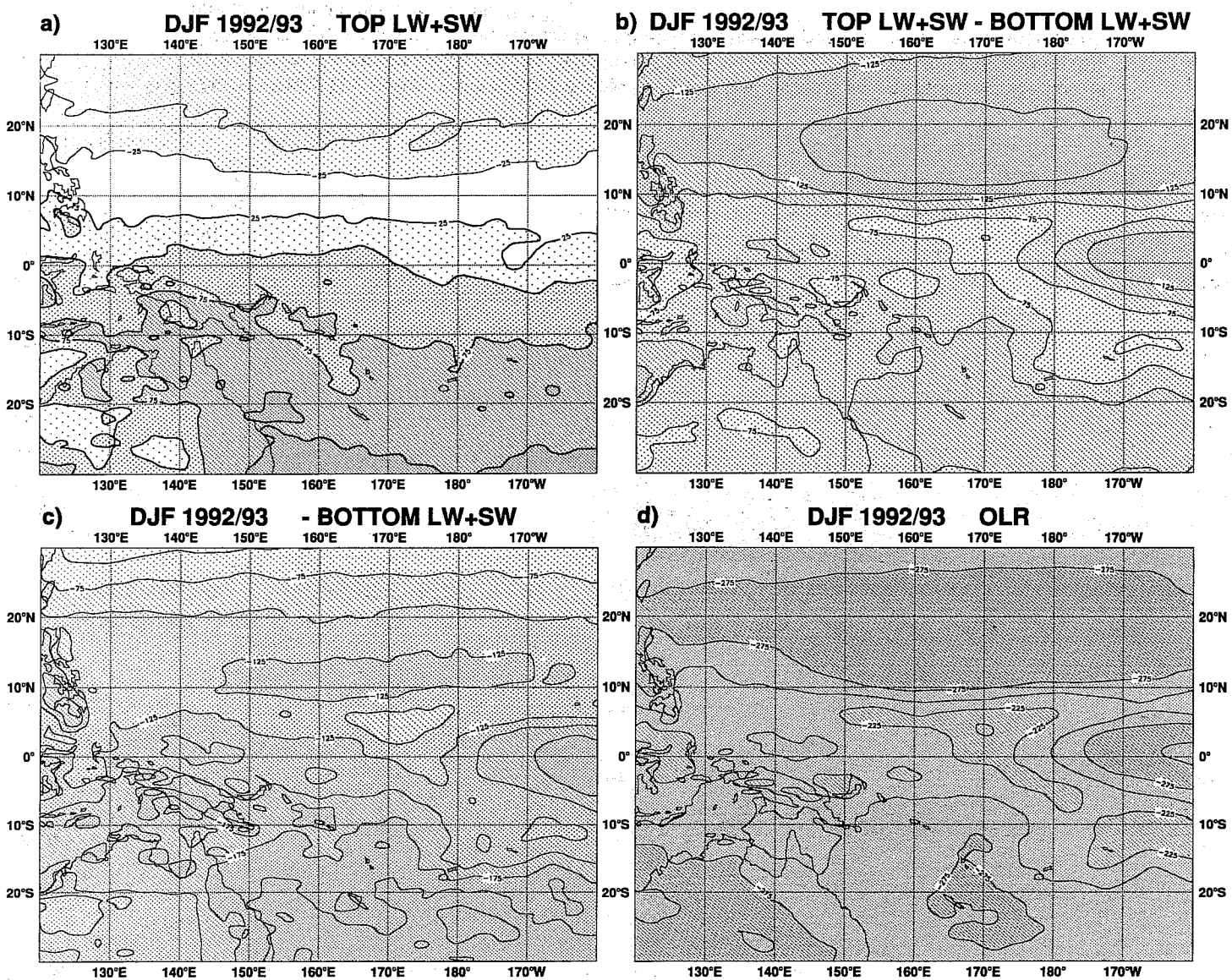

Fig 3.4 Single terms of the radiative budget for DJF 1992/93 accumulated over the first 24 hours of operational forecasts. Net radiation at the top of the atmosphere (a), net radiative flux divergence of the atmosphere (b), net radiation at the surface (c), net long-wave radiation at the top of the atmosphere (d). Sign convention: positive values represent gain of energy for the atmosphere. Units: W/m^2.

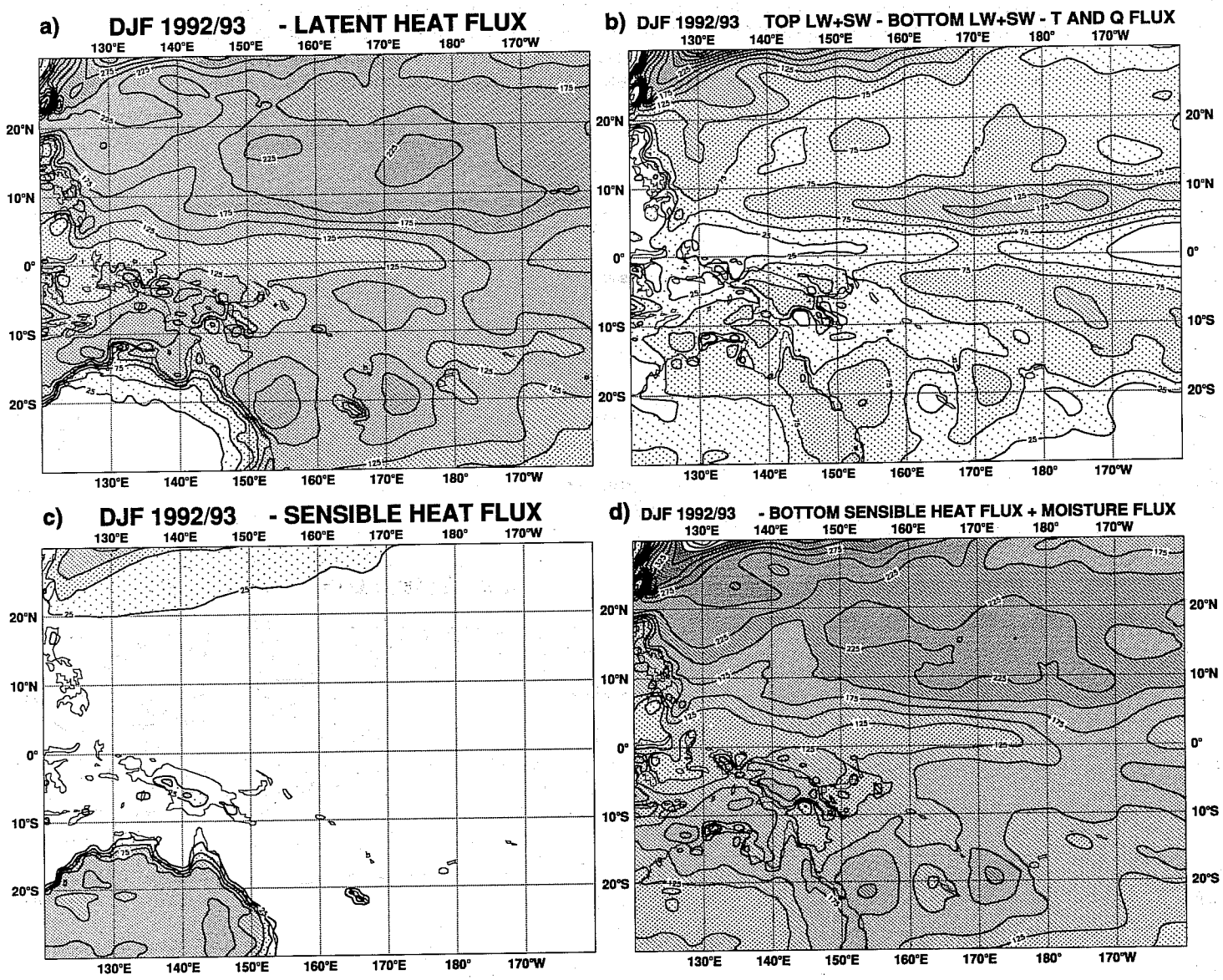

Fig. 3.5 Overall energy budget terms and surface energy budget of DJF 1992/93 accumulated over the first 24 hours of operational forecasts. Surface latent heat flux (a), net gain of energy for the atmosphere (b), surface sensible heat flux (c), net surface flux (d).Sign convention: positive values represent gain of energy for the atmosphere. Units: W/m^2.

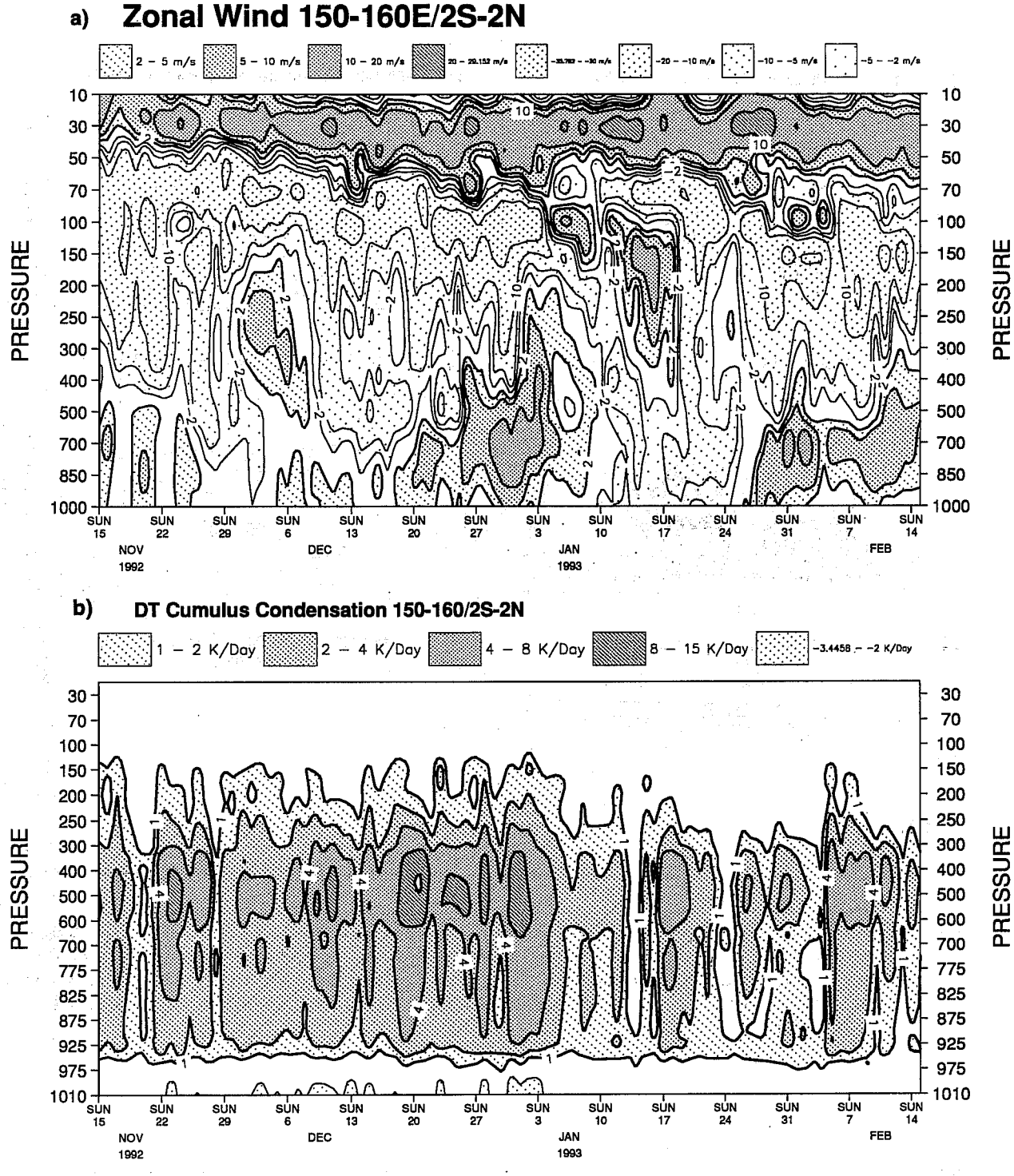

Fig. 4.1 Time-pressure cross section of the zonal wind and the diabatic heating due to cumulus convection averaged over 150E to 160E and 2S to 2N. Diabatic heating represents accumulated values over 24 hours. Units: m/s (a) and K/day (b).

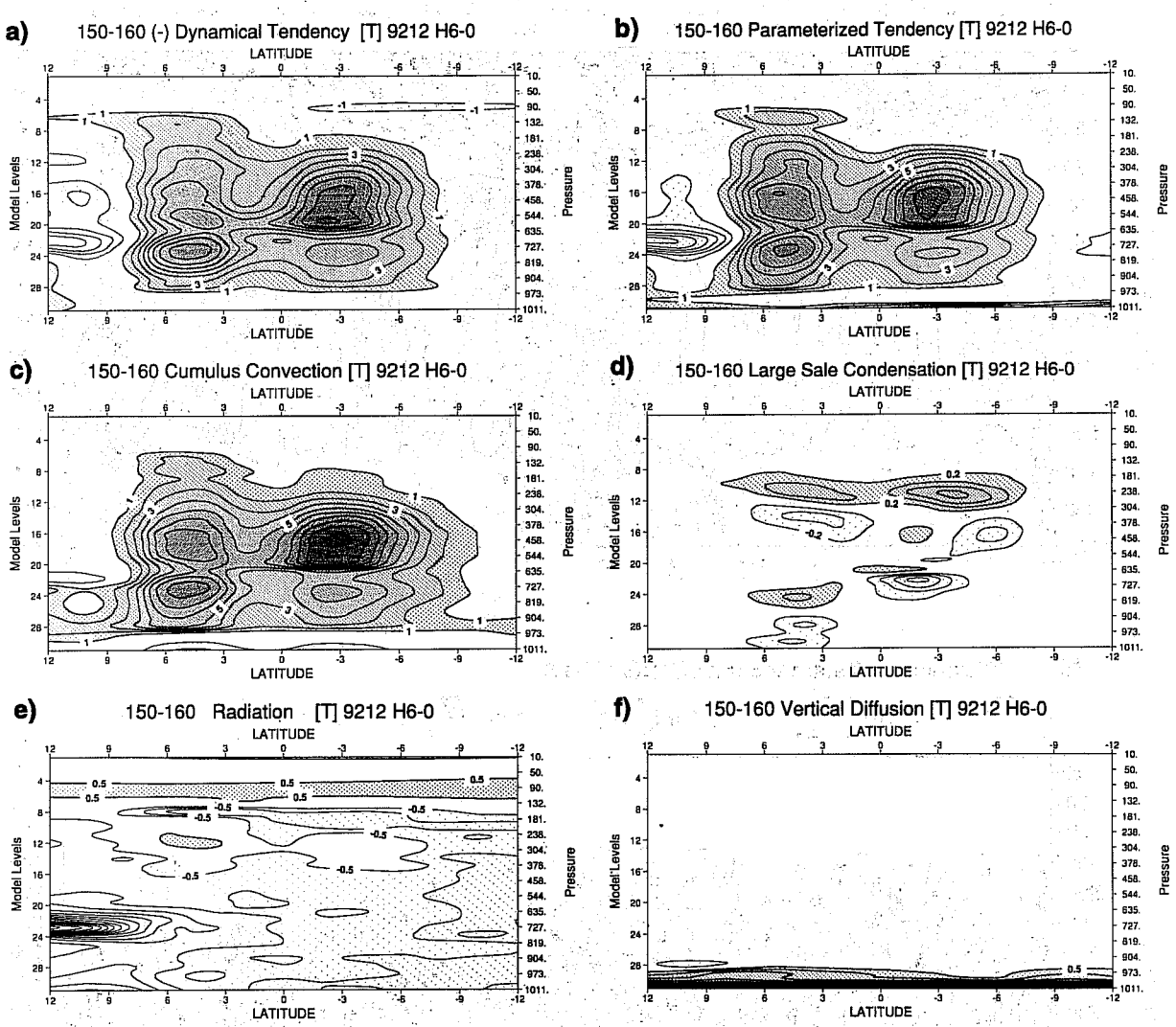

Fig. 4.2 Vertical cross section of the single terms of the heat budget averaged from 150E to 160E. The budget terms represent accumulated six hour tendencies averaged over 4 cases per day for the third week in December 1992. Dynamical tendencies with negative sign (a), parameterized tendencies (b). Diabatic forcing due to cumulus convection (c), due to large scale convection (d), due to radiation (e), due to vertical diffusion (f). Units: K/day

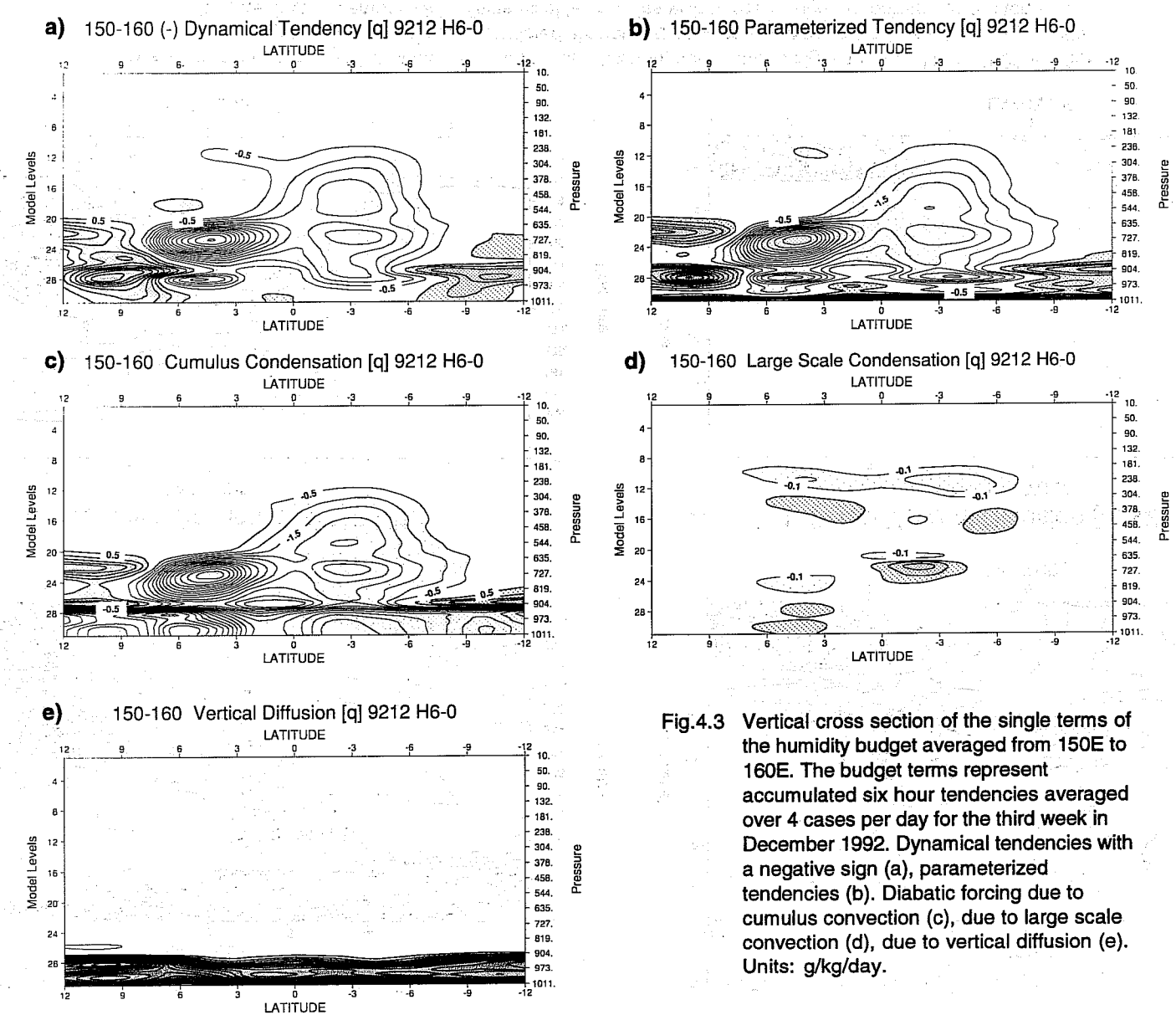

Fig.4.3 Vertical cross section of the single terms of the humidity budget averaged from 150E to 160E. The budget terms represent accumulated six hour tendencies averaged over 4 cases per day for the third week in December 1992. Dynamical tendencies with a negative sign (a), parameterized tendencies (b). Diabatic forcing due to cumulus convection (c), due to large scale convection (d), due to vertical diffusion (e). Units: g/kg/day.

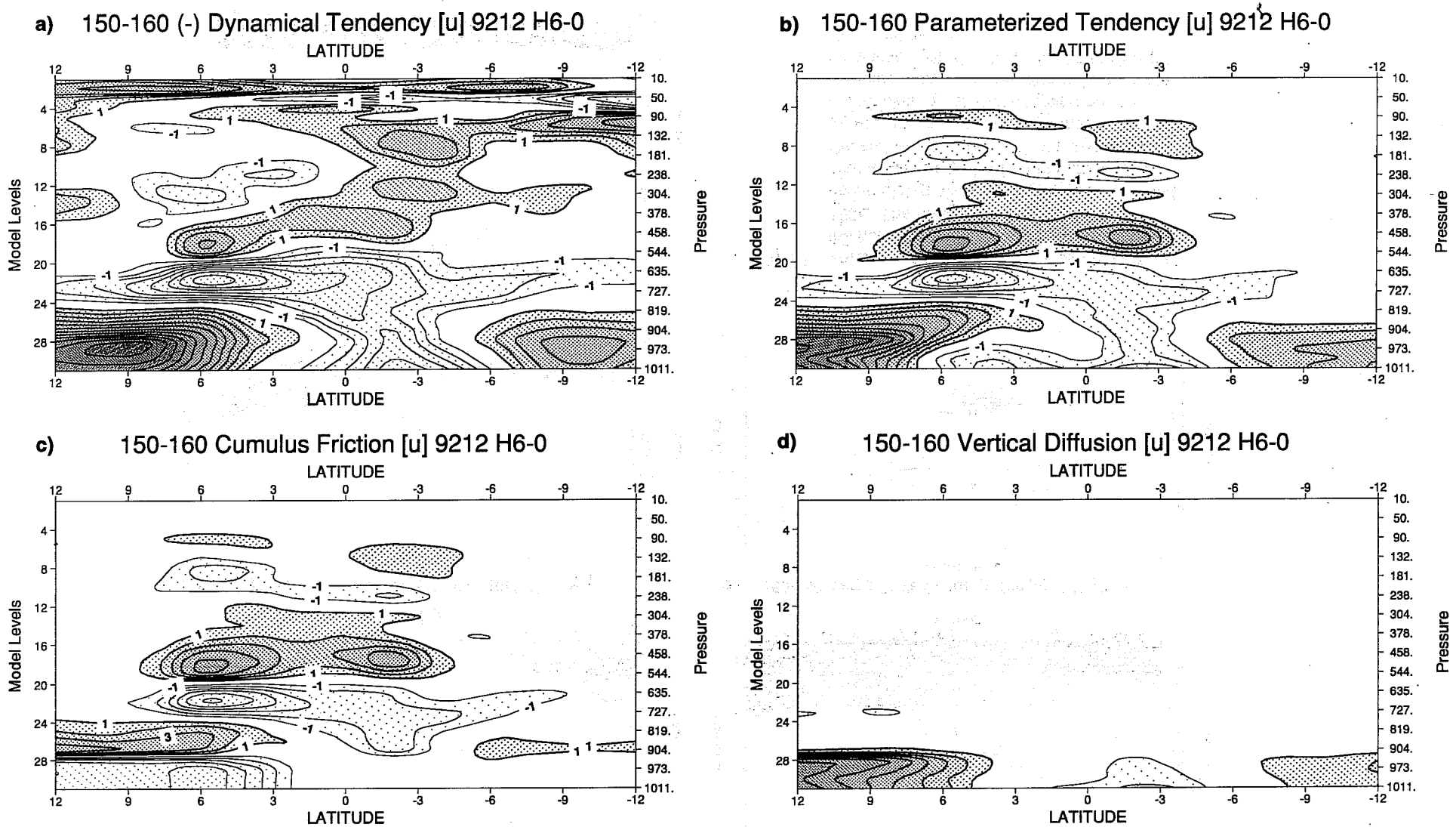

Fig. 4.4 Vertical cross section of the single terms of the zonal momentum budget averaged from 150E to 160E. The budget terms represent accumulated six hour tendencies averaged over 4 cases per day for the third week in December 1992. Dynamical tendencies with negative sign (a), parameterized tendencies (b). Diabatic forcing due to cumulus convection (c), due to vertical diffusion (d). Units: m/s/day